Supplementary Material (ESI) for Chemical Communications
This journal is (c) The Royal Society of Chemistry 2007

Supplementary Data

1. Sample Preparation

The aligned carbon nanotube (ACNT) samples were prepared in a tubular CVD reactor. The reactor consisted of a quartz tube spanning through a low-temperature section (Zone I) and a high-temperature section (Zones II), respectively. The input CVD precursor contained 0.975 g ferrocene dissolved into 10 ml o-xylene (both from Sigma-Aldrich). The precursor was injected and vaporized at the reactor Zone I with T = 225 °C by a pump at a feeding rate of 0.21 ml/min. Ar/H_2 gas mixture was used to transport the vaporized precursor from Zone I to Zone II. Vertically aligned multiwalled carbon nanotubes formed on the surface of quartz plates positioned in the Zone II with T = 725 °C. For nitrogen doped sample ACNT-1, 15% ammonia was added into the gas mixture. The precursor solution was supplied for 10 minutes before it was stopped. After being cooled down to room temperature in H_2/Ar flow, the quartz plates with ACNT were taken out and sealed in air-tight container.

2. Electrochemical Characterization

2.1 Activity Study:

In addition to CV data reported in the main text, the catalytic activity of functionalized carbon nanotubes was also investigated using the steady-state cyclic potential sweeps over a rotating disk electrode (RDE). The nanotubes are highly graphitic and can not be attached directly on the disk surface of the glassy carbon electrode. Therefore a catalyst inks had to be prepared by adding small amount of Nafion® ionomer to assist the attachment. The inks were prepared by mixing the catalyst with 5wt.% Nafion® solution in the weight ratio of 7/3 (Catalyst/Nafion®). Isopropanol was used as the dispersion medium. The suspension was stirred (magnetic) for at least 12 hours to obtain a smooth paste. A thoroughly polished glassy carbon disk electrode (0.196 cm^2 surface area) was used to support the catalyst. The smooth catalyst ink was pipetted onto the glassy carbon and air dried. Typically 0.1 mg catalyst was deposited on the electrode for RDE test (for both ACNT-1 and ACNT-2)

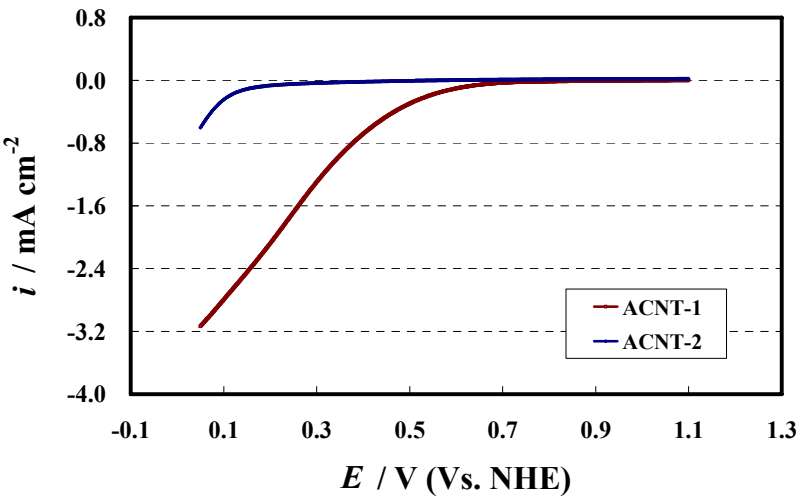

Figure 1. The cathodic sweeps over RDE of ACNT-1 and ACNT-2 measured in O_2 saturated electrolyte (0.6 M $HClO_4$) after subtracting the O_2-free background obtained by purging electrolyte with Argon.

Electrochemical measurements were recorded in a jacketed one-compartment, 3-electrode cell using a RDE unit (Pine Instruments), a speed controller (Pine Instruments), and a PC interfaced bipotentiostat (CH Instruments). The electrolyte used was 220 ml 0.6 M $HClO_4$, kept at ambient temperature. It was prepared by adding high purity water from Milli-Q plus system (18 MΩ) to double distilled 70 % $HClO_4$ (GFS Chemicals), followed by purging with Ar for 30 minutes prior to use. Coiled Pt wire was used as counter electrode. Hg/Hg_2SO_4 (0.5M H_2SO_4) was used as reference electrode. Figure 1 shows the cathodic sweeps produced from the steady-state CVs for ACNT-1 and ACNT-2 in the oxygen saturated electrolyte after subtracting the backgrounds obtained in oxygen free environment by sparging with Ar. The potential limits for the CV were set from 0 to 1.1 volts and the scan rate was controlled at 10 mV/sec. The rotating speed was kept at 1600 rpm during the study. The results clearly reconfirmed that N-doped ACNT-1 has substantially higher catalytic activity and onset potential for ORR than that of ACNT-2.

2.2 Stability Study:

To verify if the FeN_4 active site in the nanotube is sustainable in the strong acidic environment and to remove any concern that the observed ORR activity may arise from the reaction of contamination species, we conducted a chronoamperometric study for ACNT-1 in the oxygen saturated electrolyte (0.6 M $HClO_4$) at RDE speed of 1600 rpm. Two consecutive measurement cycles were made where each one lasted one hour. For each cycle, the electrode potential was set at 0.43 volts (NHE) for the first half hour and 0.23 volts for the second half hour. Both are below the ORR onset potential (0.79 Volt). The electrode current as a function of the elapsed time is plotted in Figure 2. It was observed that the current re-established itself relatively fast and approached gradually to equilibrium after each potential step change. Furthermore, the measurement of cycle 2 almost duplicated that of cycle 1, suggesting that the catalyst has an excellent acid tolerance and the electrocatalytic reaction was not attributed to any surface contamination.

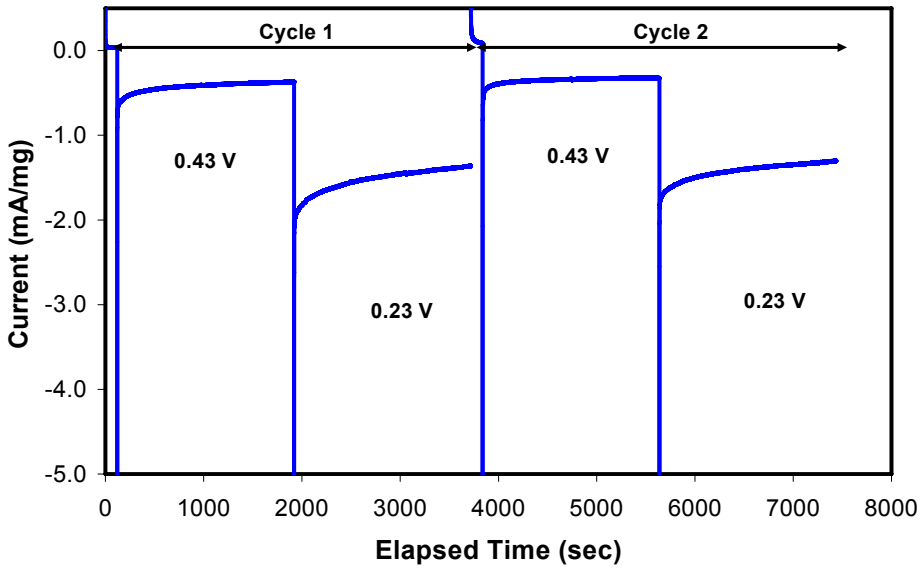

Figure 2. Chronoamperometric measurement of ACNT-1in an oxygen saturated $HClO_4$ solution (0.6M). RDE rotating speed = 1600 rpm.

We also evaluated the catalyst's acid tolerance in longer term by measuring CV's of ACNT-1 coated electrode after it had been immersed in the oxygen saturated electrolyte (0.6 M $HClO_4$) for up to six days, as are shown in Figure 3. The measurement condition was identical to that reported in the main text. Little change was observed between the first and second day's measurement. Small shifts in the cathodic peak intensity and potential were observed in the measurement of the sixth day. This change can be partially attributed to the degradation of the electrode by loss of material through minor spallation.

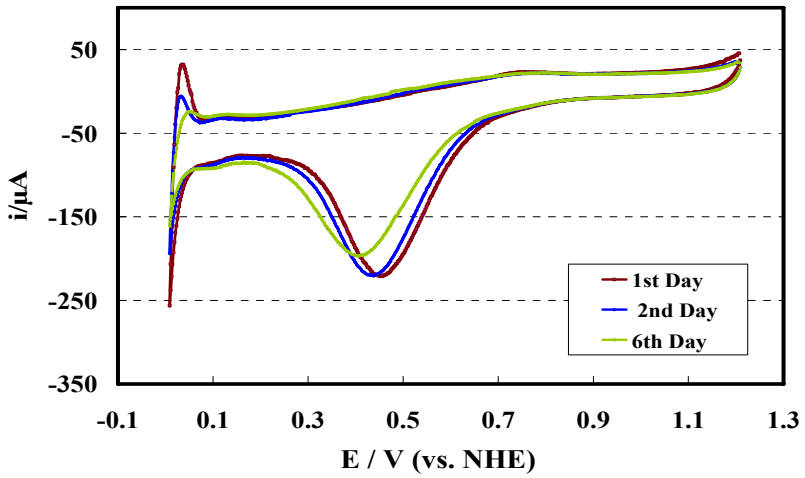

Figure 3. CVs for ACNT-1 measured in 0.6 M $HClO_4$ electrolyte saturated with oxygen in different days

3. X-Ray Absorption Data Acquisition and Analysis

X-ray absorption spectroscopy (XAS) measurement at the energy of Fe K-edge (7.112 KeV) was carried out at Beamline 12 BM of Advanced Photon Source at Argonne National Laboratory. The X-ray beam was focused through a Pt-coated mirror which also removed higher harmonic fraction of the photons. A typical beam size at the surface of the sample was 1.0 mm (horizontal) and 0.5 mm (vertical). A feedback loop with 70% detuning was used to control the monochromator crystal for higher harmonic rejection. A multiple-element germanium solid-state detector (Canberra) was used to collect K_α X-ray fluorescence signals from Fe in the carbon nanotube samples. To further enhance the signal-to-noise ratio, a manganese filter was placed in front of the detector for attenuation of elastic scattering from the Fe K-edge. The outputs from the amplifiers of the detector were connected to a group of single channel analyzers (SCA) with proper upper and lower thresholds to allow only $K_{\alpha 1}$ and $K_{\alpha 2}$ fluorescence signals of Fe to be further processed. An ion chamber was placed before the sample for the X-ray flux reference signal (I_0). A second and a third ion chambers were placed after the sample for the transmission (I_t) and reference (I_f) signal measurements, respectively. An iron foil was inserted between the second and the third ion chambers and was used for X-ray photon energy calibration. The output signals from the SCA's were connected to a scaler array which was interfaced with a data acquisition computer.

Thin layers of ACNT samples were transferred from the CVD substrate onto a polyimide tape through a press-and-peel method and were air tightly sealed. The Fe content in ACNT layer was relatively low corresponding to X-ray absorption of ~ 10^{-3} above the K-edge threshold.

Conventional XAS data analysis programs, WinXAS (T. Ressler) and FEFF8 (University of Washington) were used in data analysis and simulation of the spectra of the ACNT samples. Fe foil and iron(II) phthalocyanine were used as the reference compounds for the structural parameters and the FEFF calculations. Selected single scattering paths were used to extract the amplitude and the phase parameters of Fe and N back-scatterings from the nearest neighbors, and those parameters were used in subsequent fittings based on the equation:

$$\chi(k) = \sum F_i(k)\, S_0^2(k)\, N_i /(kR_i^2) exp(-2\sigma_i^2 k^2) sin[2kR_i+\delta_i(k)] \qquad (1)$$

where $F(k)$ is the magnitude of the backscattering, S_0, amplitude reduction factor, N, the coordination number, R, the average distance, σ, the Debye-Waller factor, and δ, the phase shift; the subscript indicates ith atom; k is the electron wavevector[1]. The Fe-N and Fe-Fe bond lengths in ACNT were obtained from the fits using the parameters derived from the reference compounds using the single scattering path model. The k spans of the Fourier transformation were kept nearly the same for all samples in the ranges from 3 up to 15 $Å^{-1}$.

Shown in Figure 4 are the XANES spectra of ACNT-1 and ACNT-2. XANES for ACNT-2 resembles to a typical spectrum of highly dispersed iron metallic particle[2] which is also consistent with both EXAFS and SEM results discussed in the main text. The XANES spectrum for ACNT-1 indicates that there are at least two types of iron compounds, one of which is iron particles at zero-valence state Fe^0, as is shown by the X-ray absorption transition at ΔE = 0 eV where $\Delta E = E - E_0$; E is the X-ray photon energy and E_0 is the K-edge threshold energy, respectively. The metal particle contribution to the XAS spectrum of ACNT-1 can be removed through a fractional subtraction method until Fe^0 threshold peak at ΔE = 0 eV is reduced to zero. Our analysis using this method identified ~55% of iron in ACNT-1 is in the form of Fe micro-crystallite. The XANES spectrum after the subtraction of Fe^0 contribution revealed that the remaining Fe moiety has the feature of iron (II) coordinated by four nitrogen atoms inside of a macrocyclic structure with a square-planar configuration, as is shown in Figure 4 of the main text.

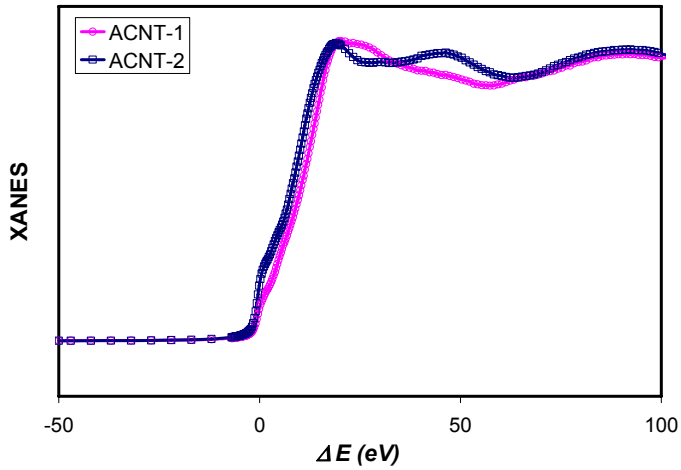

Figure 4. XANES spectra of ACNT-1 and ACNT-2

Fourier transformation of EXAFS spectra were analyzed using the single scattering path method previously mentioned. For ACNT-2, only Fe-Fe interaction was observed. The fitting of the coordination structure with Fe foil as reference yielded N = 4.5, R = 2.56 Å and $\sigma = 1.0\text{x}10^{-2}$, respectively. For ACNT-1, both Fe-N and Fe-Fe interactions were observed at different shell distances. The former was from the active site and the latter was from metal crystallites. The

EXAFS simulation on the active site was carried out either through a simultaneous fitting using a two-shell model or using an one-shell model after the subtraction of Fe particle contribution from $\chi(k)$. Both approaches led to a similar result with the coordination structure of $N = 4.2$, $R = 1.95$ Å and $\sigma = 3.2\text{x}10^{-3}$ for Fe-N shell, respectively. Shown in Figure 5 is the comparison of the experimental data and the simulation when a two-shell model was used. Excellent fit was observed.

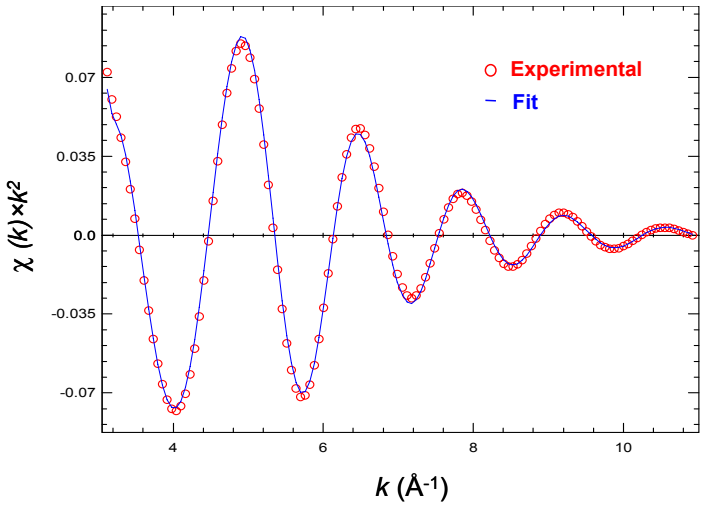

Figure 5. The comparison of the experimental χ function derived from EXAFS spectrum of ACNT-1 and simulation results from a two-shell model.

4. TEM Study

Figure 6 shows a typical TEM image of ACNT-1 taken at the iron particle-free region. No discernable Fe microcrystallites were observed. Meanwhile, EDS analysis on the same region found the co-existence of Fe and N, presumably as the atomically embedded species, as is given in Table I.

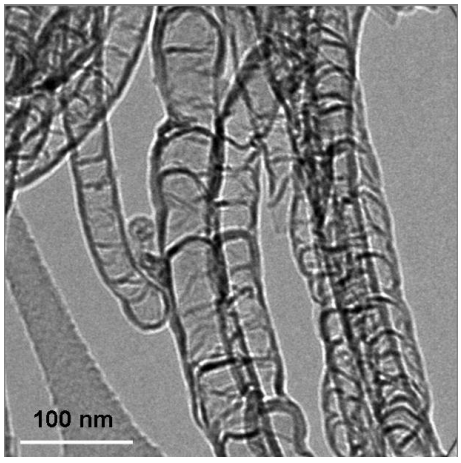

Figure 6. TEM image of ACNT-1 in metal particle-free region.

Table I. EDS data on the elemental distribution in metallic particle free region.

Element	Weight %	Atomic %
C K	96.5	97.3

N K	1.8	1.6
Fe K	0.4	0.1

5. Metallic Fe Inside of ACNT

During the preparation and characterization of ACNT, we found that a fraction of metallic iron always remained inside of the carbon nanotubes that can not be removed by the conventional chemical treatment. For example, we could still detect a significant fraction of metallic iron through EXAFS after the sample had been immersed and washed by the concentrated H_2SO_4 or HNO_3 for 4 days. Our TEM study showed that these iron crystallites were encapsulated inside of the nanotubes, as is shown in Figure 7, therefore will not participate the electrochemical reaction or be leached out during fuel cell operation.

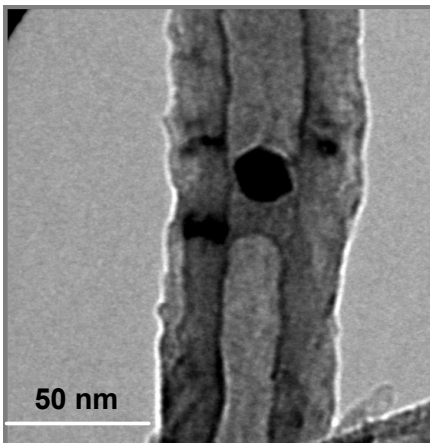

Figure 7. TEM image of an iron particle encapsulated inside of a nanotube

Reference:
1. D. C. Koningsberger and R. Prins, X-ray Absorption: Principles, Applications, Techniques of EXAFS, SEXAFS and XANES; John Wiley & Sons Inc.: Chichester UK, 1988.
2. H. Purdum, P. A. Montano, G. K. Shenoy and T. Morrison, Phys. Rev. B 1982, **25**, 4412.